Performance Evaluation of THz Wireless Systems Operating in $275 - 400$ GHz Band

Alexandros-Apostolos A. Boulogeorgos*, Evangelos N. Papasotiriou*, Joonas Kokkoniemi, Janne Lehtomäki†, Angeliki Alexiou*, and Markku Juntti†

*Department of Digital Systems, University of Piraeus, Piraeus 18534, Greece. E-mails: al.boulogeorgos@ieee.org, {vangpapasot, alexiou}@unipi.gr

†Centre for Wireless Communications (CWC), University of Oulu, 90014 Oulu, Finland. E-mail: joonas.kokkoniemi, markku.juntti, janne.lehtomaki@oulu.fi

***Abstract*—In this paper, we establish the appropriate system model for the terahertz (THz) wireless link in the range of 275 to 400 GHz, which accommodates the channel particularities and transceivers parameters. The channel particularities include the frequency selectivity, pathloss, as well as the atmospheric conditions, namely temperature and pressure, while the transceiver parameters, which are taken into account, are the antenna gains as well as the power allocation of the transmitted signal. Moreover, we present analytical expressions, with low computational complexity, for the evaluation of the average SNR, and capacity for line of sight wireless THz links. These expressions are expected to be the key tools for the design of the THz link.**

I. Introduction

The increased data rates demand, in the beyond fifth generation (5G) wireless systems, as well as the fact that the spectral efficiency of the microwave links is approaching its fundamental limits have motivated the exploitation of higher frequency bands that offer abundance of communication bandwidth [1], [2]. Towards this end, terahertz (THz) band wireless communications have been recognized as an attractive canditate for providing an order of magnitude capacity improvements [3]–[5].

Although THz communications can benefit from an extreme increase in the bandwidth, it comes at the price of suffering severe path loss, which drastically limits the links range [5], [6]. To overcome this problem, a great amount of research effort has been put on modeling the particularities of the THz channel [7]–[11]. For instance, in [7], the authors presented an initial path-loss model for nano-sensor networks, that describes the THz propagation behaviour through plant foliage, whereas, in [8], a channel model for intrabody nanoscale communications was provided. Additionally, in [10], a model, which evaluates the total absorption loss assuming that the propagation medium is the air, natural gas and/or water, was proposed. In [11], the authors presented a multi-ray THz model for THz communications. All the published results agrees on the fact that THz communication channel has a strong dependence on both the molecular composition of the medium and the transmission distance.

The results of these models were capitalized in [12]–[14], where performance metrics for the THz link effectiveness was presented. In more details, in [12], the authors analyzed the THz link capacity in electromagnetic nano-sensor networks, while, in [13], the authors conducted a throughput analysis in THz nano-sensor networks and revealed that there exist a relation between the transparency windows and the transmission distance. Additionally, in [14], the basic properties of THz-waves was investigated and the maximum achievable data rates for fixed wireless THz-links was evaluated. Finally, in [15], the authors analyzed the THz channel behavior in order to design reconfigurable multiple input multiple output systems. In all of the mentioned works, the channel models that are based on the high-resolution transmission molecular absorption (HITRAN) database to accommodate the impact of the molecular absorption loss, have been used. As a consequence, it is difficult to evaluate the THz link performance as well as to provide the appropriate design guidelines and tools.

Motivated by the above, in this paper, we provide the mathematical framework to evaluate and quantify the performance of the THz link in the 275–400 GHz band. In particular, by employng a simplified, but accurate, model, which was initially presented in [16], we provide novel easily-computed analytical expressions for the average SNR, and capacity for line of sight (LoS) THz links in the range of $275 - 400$ GHz. These expressions reveal how the performance of the THz system depends on the transmission environment, the communication bandwidth, the distance between the transmitter (TX) and the receiver (RX) and the gain of the TX and RX antennas. As a result, they can play a significant role as design tools for THz wireless systems.

The remainder of this paper is organized as follows. In Section II, the system and channel models are described, whereas, in Section III, the analytical metrices for the evaluation of the average signal to noise ratio (SNR), and capacity are provided. Additionally, respective numerical and simulation results are given in Section IV accompanied by an insightful discussion. Finally, Section V concludes the paper by summarizing out main findings.

II. System and Channel Model

In this section, we present the system model. In more detail, in Section II-A, the signal model and the assumption of our analysis are provided, whereas, in Section II-B, the channel model for the 275–400 band is presented.

A. Signal Model

We assume that a transmitted signal, s, is emitted over a THz wireless channel, h, with an additive white Guassian noise (AWGN), n. The received radio frequency (RF) signal is passed through various processing stages, also known as the RF front-end of the RX. These stages include filtering, amplification, analog in-phase and quadrature (I/Q) demodulation, down-conversion to baseband and sampling. To this effect, the corresponding baseband equivalent received signal can be expressed as

$$r = h * s + n, \tag{1}$$

where $*$ represents the convolution operator, while h denotes the channel coefficient and n represents the zero-mean circularly symmetric complex AWGN with single-sided power spectrum densities (PSD) of N_0. It is assumed that the TX and RX experience line of sight (LoS) and, since scattering at the THz band induces more than 20 to 30 dB attenuation, i.e., only the LOS component can be used for reliable high data rate transmission, without loss of generality, the non-LoS components can be neglected [17]–[19]. Moreover, it is assumed that in order to countermease the severe pathloss of the THz channel, both of the TX and RX employ analog beamforming.

According to (1) and based on the Parseval's theorem, the signal power at the receiver, P_r, of a transmited signal with single-side power spectral density (PSD) $S(f)$ and bandwidth B, can be obtained as [9], [20]

$$P_r = \int_B S(f)|H(f,d)|^2 \mathrm{df}, \tag{2}$$

where f stands for the frequency, d is the distance between the TX and RX, and

$$H(f,d) = H_c(f,d)H_r(f), \tag{3}$$

with $H_c(f,d)$, $H_r(f)$ respectively representing the THz-band channel frequency response and the receiver frequency response. By considering an ideal low-pass filter with bandwidth B, (2) can be simplified to

$$P_r^i = \int_B S(f)|H_c(f,d)|^2 \mathrm{df}, \tag{4}$$

or, equivalently

$$P_r^i = \int_B S(f)L(f,d) \mathrm{df}, \tag{5}$$

where $L(f,d)$ denotes the total path gain. Note that for the transmitted signal PSD different distributions can be adopted. For instance, in the simplest case, it can be flat, i.e.,

$$S_f(f) = \begin{cases} S_0, & \text{for } f \in B, \\ 0, & \text{elsewhere} \end{cases}, \tag{6}$$

where S_0 is constant. Alternatively, the transmitted signal PSD can be optimally defined to maximize the channel capacity, subject to the constraint that the total transmitted power is finite. In this scenario, the PSD satisfies the water-filling principle, and can be obtained as [21]

$$S_{\mathrm{opt}}(f) = \begin{cases} K - \frac{N_0}{L(f,d)}, & \text{for } K > \frac{N_0}{L(f,d)} \\ 0, & \text{elsewhere} \end{cases}, \tag{7}$$

where K is a constant whose value depends on the total transmitted power. Note that, from (7), it is evident that the optimal transmission signal PSD takes into account the THz channel path gain.

B. Channel Model

The channel model utilized in this paper comprises of the free space path loss and molecular absorption gain, i,e, the total path gain can be evaluated as

$$L(f,d) = L_f L_a, \tag{8}$$

where L_f and L_a respectively represents the free space and molecular absorption path gains.

The free space path gain can be evaluate, by radially expanding wavefront adjusted with the RX and TX antenna gains, as

$$\mathrm{L_f} = \frac{c^2}{(4\pi df)^2} G_{\mathrm{t}}(\Theta_i) G_{\mathrm{r}}(\Theta_r), \tag{9}$$

where $G_{\mathrm{t}}(\Theta_i)$ and $G_{\mathrm{r}}(\Theta_r)$ represent the TX and RX antenna gain, respectively, and c is the speed of light. Note that the TX and RX antenna gains are usually dependent on the angles of incident Θ_i and reception Θ_r. By assuming that the TX and RX are aligned, we get that $G_{\mathrm{t}}(\Theta_i) = G_t$ and $G_{\mathrm{r}}(\Theta_r) = G_r$.

The advantage of the free space gain model is the possibility to adjust it with additional loss components in order to take into account various propagation phenomena in non-idealistic environments by multiplying their gain coefficients to the free space coeffcient. One such phenomenon is the molecular absorption loss in the millimeter and THz frequency regions, which can be modeled according to the Beer-Lambert's law as [12]

$$\tau(f,d) = \frac{P_{\mathrm{r}}(f,d)}{P_{\mathrm{t}}(f)} = e^{-\kappa_{\mathrm{a}}(f)d}, \tag{10}$$

where $\tau(f,d)$ stand for the transmittance, $P_{\mathrm{t}}(f)$ represents the transmitted powers, and $\kappa_{\mathrm{a}}(f)$ denotes the absorption coefficient describing the relative absorbing area of the molecules in the medium per unit volume. The main cause of absorption loss in millimeter and THz frequencies is the water vapor that causes discrete, but deterministic loss to the signals in the frequency domain. Other molecules, such as oxygen, also cause some level of loss to the signals, but the water vapor dominates the overall molecular absorption loss above 200 GHz frequencies.

In order to evaluate the absorption loss, we utilize a simplified model for the molecular absorption loss in 275–400 GHz band initially presented in [16]. According to this model, the absorption coefficient can be evaluated as,

$$\kappa_{\mathrm{a}}(f) = y_1(f,\mu) + y_2(f,\mu) + g(f), \tag{11}$$

whereas, based on (10) and (11), the molecular absorption gain can be estimated as

$$\mathrm{L_a}(f,d,\mu)=\exp(-d(y_1(f,\mu)+y_2(f,\mu)+g(f))), \quad (12)$$

where μ denotes the volume of the mixing ratio of water vapor. Note that the volume of the mixing ratio of water vapor is not equal to its relative humidity and it can be evaluated as

$$\mu=\frac{\phi}{100}\frac{p_w(T,p)}{p}, \quad (13)$$

where ϕ and p respectively stand for the relative humidity and the pressure, whereas $p_w(T,p)$ is the saturated water vapor partial pressure in temperature, T, and can be calculated according to Buck equation [22]. Moreover, the parameters $y_1(f,\mu)$, and $y_2(f,\mu)$, and $g(f)$ of (12) can be expressed as

$$y_1(f,\mu)=\frac{A(\mu)}{B(\mu)+\left(\frac{f}{100c}-c_1\right)^2}, \quad (14)$$

$$y_2(f,\mu)=\frac{C(\mu)}{D(\mu)+\left(\frac{f}{100c}-c_2\right)^2}, \quad (15)$$

and

$$g(f)=p_1f^3+p_2f^2+p_3f+p_4, \quad (16)$$

where $c_1=10.835\ \mathrm{cm}^{-1}$, $c_2=12.664\ \mathrm{cm}^{-1}$, $p_1=5.54\times10^{-37}\ \mathrm{Hz}^{-3}$, $p_2=-3.94\times10^{-25}\ \mathrm{Hz}^{-2}$, $p_3=9.06\times10^{-14}\ \mathrm{Hz}^{-1}$, $p_4=-6.36\times10^{-3}$, and

$$A(\mu)=0.2205\mu(0.1303\mu+0.0294), \quad (17)$$

$$B(\mu)=(0.4093\mu+0.0925)^2, \quad (18)$$

$$C(\mu)=2.014\mu(0.1702\mu+0.0303), \quad (19)$$

$$D(\mu)=(0.537\mu+0.0956)^2. \quad (20)$$

This model was shown to have high accuracy for up to $1\ \mathrm{km}$ links in standard atmospheric conditions, i.e., temperature of $296\ ^{\circ}\mathrm{K}$ and pressure of $101325\ \mathrm{Pa}$ [16]. Moreover, since the impact of the temperature and pressure can be modeled through the water vapor mixing ratio, μ, (12) can describe the THz link molecular absorption pathloss beyond the standard atmospheric conditions. Finally, note that the parameters c_1, c_2, p_1, p_2, p_3, and p_4 can be considered relatively independent of the atmospheric conditions [16][1].

Based on (8), (9), and (12), the total path gain can be rewritten as

$$L(f,d,\mu)=\frac{c^2}{(4\pi df)^2}G_{\mathrm{t}}G_{\mathrm{r}} \times\exp(-d(y_1(f,\mu)+y_2(f,\mu)+g(f))). \quad (21)$$

From (21), it is evident that the total pathloss depends not only on the operation frequency, f, and the distance between the TX and RX, but also on the TX and RX antenna gains, as well as the atmospheric conditions.

[1]More details on the molecular absorption model, which is described by (12), and its derivations can be found in [16].

III. Performance Evaluation

In order to quantify the potential of the THz band for wireless communications, in this section, we present fundamental link quality performance metrics, namely, SNR, and capacity.

A. SNR

According to (1), the SNR can be expressed as

$$\gamma(f,d,B,\mu)=\frac{P_r^i}{BN_0}. \quad (22)$$

By substituting (5) into (22), SNR can be equivalently rewritten as

$$\gamma(f,d,B,\mu)=\frac{\int_B S(f)L(f,d)\mathrm{df}}{BN_0}, \quad (23)$$

or, by using (21), as

$$\gamma(f,d,B,\mu)=\frac{c^2}{(4\pi d)^2}\frac{G_{\mathrm{t}}G_{\mathrm{r}}}{BN_0}\mathcal{I}(f,B), \quad (24)$$

where

$$\mathcal{I}(f,B)=\int_{f-\frac{B}{2}}^{f+\frac{B}{2}}\frac{S(f)}{f^2}\exp(-d(y_1(f,\mu)+y_2(f,\mu)+g(f)))\mathrm{df}. \quad (25)$$

B. Capacity

Since, the THz channel is highly frequency-selective, and under the common assumption that the transmitted signal and the total noise are jointly Gaussian, the capacity, C, of a transparency windows in the THz band can be estimated by employing the classic Shannon result for coherent reception as [13]

$$C=\int_B\log_2\left(1+\tilde{\gamma}(f,d)\right)\mathrm{d}f, \quad (26)$$

where

$$\tilde{\gamma}(f,d)=\frac{S(f)L(f,d)}{N_0}. \quad (27)$$

From (24) and (26), it is evident that the SNR and achievable capacity depend not only on the transmission distance, the noise PSD and the bandwidth, but also on the power allocation scheme, which will be selected, as well as the atmospheric conditions.

IV. Results and Discussion

In this section we quantitatively compare the effectiveness of the THz link in terms of SNR and capacity, assuming different transmission bandwidths, central frequencies, power allocation schemes, as well as atmospheric conditions. For the transmission distance, path lengths ranging from 0.1 to $500\ \mathrm{m}$ are considered. Furthermore, it is important to note that, unless otherwise is stated, in the following figures, the numerical results, which was derived by using the expressions of Section III, are shown with continuous lines, while markers

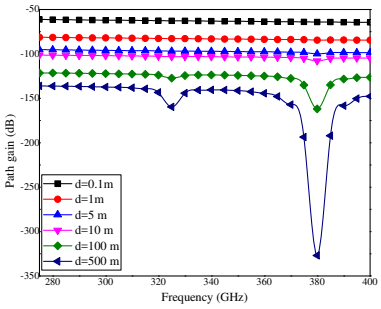

Fig. 1: Path gain as a function of the operation frequency for different transmission distances, assuming $G_t = G_r = 1$ and standard atmospheric conditions.

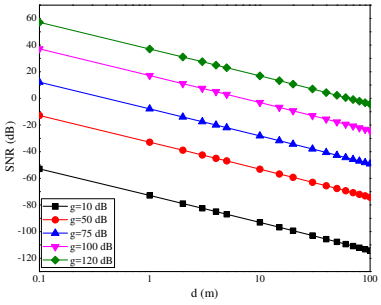

Fig. 2: SNR as a function of the distance for different values of g, assuming flat transmission signal PSD, $B = 125$ GHz and standard atmospheric conditions.

are employed to illustrate the results derived via the path gain model that employ the Beer-Lambert law [12].

Fig. 1 illustrates the path gain as a function of the frequency for different distances, assuming standard atmospheric conditions and $G_t = G_r = 1$. The results derived with the presented path gain model are identical with the results derived by the Beer-Lambert law [12]; thus, verifying the accuracy of the presented model. Moreover, from this figure, it is evident that, for a fixed transmission frequency, as the distance increases the path gain decreases. For example, for $f = 380$ GHz, as the distance alters from 0.1 to 100 m, the path gain decrease about 100%. This indicates the importance of employing beamforming schemes in order to increase the TX and RX antenna gains and countermeasure the impact of the channel losses. Additionally, we observe that the frequency selectivity due to the molecular absorption becomes more severe as the distance increases. As a result, the bandwidth of the transparency windows decreases with an increase on the transmission range. For instance, for $d = 0.1$ m, a transparency window exists in the range of 275 to 400 GHz with bandwidth equals 125 GHz. On the other hand, for $d = 100$, the range of the transparency window is from 330 to 370 GHz and its bandwidth equals 40 GHz, while, for $d = 500$ m, the corresponding window is from the range of 340 to 360 GHz. In other words, a five-fold increase in distance results in a 50% decrease of the transparency window.

Fig. 2 demonstrates the detrimental impact of pathloss due

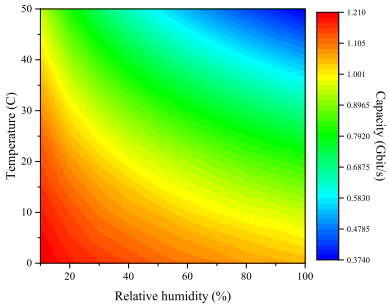

Fig. 3: Capacity as a function of the temperature and the relative humidity, for $d = 100$ m, $\frac{G_t G_r S_0}{N_0} = 100$ dB, assuming flat transmission signal PSD, $B = 125$ GHz and standard atmospheric conditions.

to the distance variation to the received signal quality. In more detail, we plot the SNR as a function of the distance for different values of $g = \frac{G_t G_r S_0}{N_0}$, assuming flat transmission signal PSD and $B = 125$ GHz. As expected, for a fixed g, as the distance increases the SNR decreases. For instance, for $g = 100$ dB, a transmission distance increase from 1 to 10 m results in a about 20 dB SNR degradation. Moreover, for a given distance, the SNR increases as g increases. For example, for $d = 50$ m, as g increases from 75 to 120 dB, the SNR also increases from -42.68 to 2.32 dB. This indicates that, for a given RX and transmission power, in order to increase the link range, someone needs to increase the gain of the TX and/or RX antennas.

Fig. 3 depicts the capacity as a function of the temperature and the relative humidity, for $d = 100$ m, $\frac{G_t G_r S_0}{N_0} = 100$ dB, assuming flat transmission signal PSD and bandwidth equals 125 GHz. As expected, for a fixed temperature, as the relative humidity increases, the channel capacity decreases. For example, for $T = 25^o C$, a 10% capacity degradation occurs, as the relative humidity alters from 60% to 90%. Moreover, for a given relative humidity, as the temperature increases, the capacity decreases. For instance, for a relative humidity equals 50%, the capacity decreases for about 53.91%, as the temperature increases from 20 to $50^o C$. This reveals that the impact of temperature variation in the THz link performance are more severe compared with the one of the humidity variations.

Fig. 4 presents the impact of the transmission signal PSD on the performance of the THz system. In particular, the capacity is plotted as s a function of the transmission distance for different transmission signal PSD and bandwidth, assuming $\frac{G_t G_r S_0}{N_0} = \frac{G_t G_r K}{N_0} = 120$ dB, and standard atmospheric conditions. As expected, for a given transmission PSD and bandwidth, as the distance increases, the capacity decreases. Moreover, for a given transmission PSD and distance, as the bandwidth increases, the capacity also increases. For example, for $d = 1$ m and optimal transmission PSD, the capacity increases about 24.2%, as the bandwidth alters from 100 to

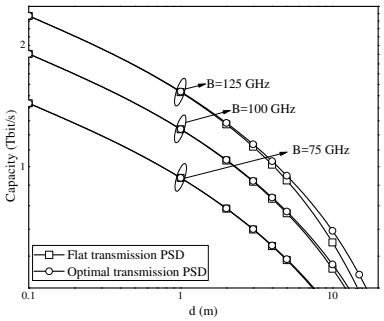

Fig. 4: Capacity as a function of the transmission distance for different transmission signal PSD and bandwidth, assuming $\frac{G_t G_r S_0}{N_0} = \frac{G_t G_r K}{N_0} = 120$ dB, and standard atmospheric conditions.

125 GHz, whereas, for $d = 10$ m and for the same bandwidth alteration, the corresponding capacity increase equals 21%. This example reveals that as the distance increases, the capacity increase due to a corresponding bandwidth increase is constraint. Additionally, from this figure, we observe that, for a fixed bandwidth, the optimal transmission PSD outperforms the flat transmission PSD in terms of capacity; especially, as the distance and the transmission bandwidth increases. For instance, for $B = 125$ GHz and $d = 5$ m, a 2.7% capacity improvement can be achieved, if the optimal transmission PSD is employed instead of the flat one, whereas, for the same bandwidth and $d = 10$ m, the corresponding capacity improvement is up to 6.85%. This indicates the importance of taking into account the channel gain, when designing the transmission power allocation scheme.

V. Conclusions

In this paper, we presented an appropriate channel and system model for THz wireless links in the range of 275 to 400 GHz, which take int account the channel particularities and transceivers parameters. Moreover, in order to evaluate the effectiveness of the THz system, we presented analytical expressions with low computational complexity for the evaluation of the average SNR and capacity. Our results reveal that the frequency selectivity of the THz channel increases, as the range of the wireless link increases, whereas, in order to achieve acceptable performance in long-range links, high-gain antennas and transmission PSD designs, which take into account the channel gain, are necessary. Finally, we observed that the THz links performance depends on the atmospheric conditions.

Acknowledgment

This work has received funding from the European Commission's Horizon 2020 research and innovation programme under grant agreement No. 761794.

References

[1] A.-A. A. Boulogeorgos, A. Alexiou, T. Merkle, C. Schubert, R. Elschner, A. Katsiotis, P. Stavrianos, D. Kritharidis, P.-K. Chartsias, J. Kokkoniemi, M. Juntti, J. Lehtomäki, A. Teixeira, and F. Rodrigues, "Terahertz technologies to deliver optical network quality of experience in wireless systems beyond 5G," *IEEE Commun. Mag.*, 2018.

[2] H. Shokri-Ghadikolaei, C. Fischione, G. Fodor, P. Popovski, and M. Zorzi, "Millimeter wave cellular networks: A MAC layer perspective," *IEEE Trans. Commun.*, vol. 63, no. 10, pp. 3437–3458, Oct. 2015.

[3] R. Piesiewicz, T. Kleine-Ostmann, N. Krumbholz, D. Mittleman, M. Koch, J. Schoebei, and T. Kurner, "Short-range ultra-broadband Terahertz communications: Concepts and perspectives," *IEEE Antennas. Propag.*, vol. 49, no. 6, pp. 24–39, Dec 2007.

[4] I. F. Akyildiz, J. M. Jornet, and C. Han, "Terahertz band: Next frontier for wireless communications," *Phys. Commun.*, vol. 12, pp. 16–32, Sep. 2014.

[5] C. Lin and G. Y. L. Li, "Terahertz communications: An array-of-subarrays solution," *IEEE Commun. Mag.*, vol. 54, no. 12, pp. 124–131, Dec. 2016.

[6] G. A. Siles, J. M. Riera, and P. G. del Pino, "Atmospheric attenuation in wireless communication systems at millimeter and thz frequencies [wireless corner]," *IEEE Antennas. Propag.*, vol. 57, no. 1, pp. 48–61, Feb. 2015.

[7] A. Afsharinejad, A. Davy, B. Jennings, and C. Brennan, "An initial path-loss model within vegetation in the THz band," in *9th European Conference on Antennas and Propagation (EuCAP)*, May 2015, pp. 1–5.

[8] H. Elayan, R. M. Shubair, J. M. Jornet, and P. Johari, "Terahertz channel model and link budget analysis for intrabody nanoscale communication," *IEEE Trans. Nanobioscience*, vol. 16, no. 6, pp. 491–503, Sep. 2017.

[9] R. Zhang, K. Yang, Q. H. Abbasi, K. A. Qaraqe, and A. Alomainy, "Analytical characterisation of the terahertz in-vivo nano-network in the presence of interference based on TS-OOK communication scheme," *IEEE Access*, vol. 5, pp. 10 172–10 181, 2017.

[10] M. A. Akkas, "Terahertz channel modelling of wireless ultra-compact sensor networks using electromagnetic waves," *IET Commun.*, vol. 10, no. 13, pp. 1665–1672, 2016.

[11] C. Han, A. O. Bicen, and I. F. Akyildiz, "Multi-ray channel modeling and wideband characterization for wireless communications in the terahertz band," *IEEE Trans. Wireless Commun.*, vol. 14, no. 5, pp. 2402–2412, May 2015.

[12] J. M. Jornet and I. F. Akyildiz, "Channel modeling and capacity analysis for electromagnetic nanonetworks in the terahertz band," *IEEE Trans. Wireless Commun.*, vol. 10, no. 10, pp. 3211–3221, Oct. 2011.

[13] P. Boronin, V. Petrov, D. Moltchanov, Y. Koucheryavy, and J. M. Jornet, "Capacity and throughput analysis of nanoscale machine communication through transparency windows in the terahertz band," *Nano Communication Networks*, vol. 5, no. 3, pp. 72–82, 2014.

[14] T. Schneider, A. Wiatrek, S. Preussler, M. Grigat, and R. P. Braun, "Link budget analysis for terahertz fixed wireless links," *IEEE Trans. Terahertz Sci. Technol.*, vol. 2, no. 2, pp. 250–256, Mar. 2012.

[15] Z. Xu, X. Dong, and J. Bornemann, "Design of a reconfigurable MIMO system for THz communications based on graphene antennas," *IEEE Trans. Terahertz Sci. Technol.*, vol. 4, no. 5, pp. 609–617, Sep. 2014.

[16] J. Kokkoniemi, J. Lehtomäki, and M. Juntti, "Simplified molecular absorption loss model for 275 – 400 gigahertz frequency band," in *Proc. European Conf. Antennas Propag.*, 2018, pp. 1–5.

[17] C. Lin and G. Y. Li, "Indoor Terahertz communications: How many antenna arrays are needed?" *IEEE Trans. Wireless Commun.*, vol. 14, no. 6, pp. 3097–3107, Jun. 2015.

[18] K. Guan, G. Li, T. Kürner, A. F. Molisch, B. Peng, R. He, B. Hui, J. Kim, and Z. Zhong, "On millimeter wave and THz mobile radio channel for smart rail mobility," *IEEE Trans. Veh. Technol.*, vol. 66, no. 7, pp. 5658–5674, Jul. 2017.

[19] S. Rajagopal, S. Abu-Surra, and M. Malmirchegini, "Channel feasibility for outdoor non-line-of-sight mmwave mobile communication," in *IEEE Vehicular Technology Conference (VTC Fall)*, Sep. 2012, pp. 1–6.

[20] N. Akkari, J. M. Jornet, P. Wang, E. Fadel, L. Elrefaei, M. G. A. Malik, S. Almasri, and I. F. Akyildiz, "Joint physical and link layer error control analysis for nanonetworks in the terahertz band," *Wireless Networks*, vol. 22, no. 4, pp. 1221–1233, May 2016.

[21] J. M. Jornet and I. F. Akyildiz, "Channel capacity of electromagnetic nanonetworks in the terahertz band," in *IEEE International Conference on Communications*, May 2010, pp. 1–6.

[22] O. A. Alduchov and R. E. Eskridge, "Improved magnus form approximation of saturation vapor pressure," *J. Appl. Meteor.*, vol. 35, no. 4, pp. 601–609, Apr. 1996.